

Manuscript version: Author's Accepted Manuscript

The version presented in WRAP is the author's accepted manuscript and may differ from the published version or Version of Record.

Persistent WRAP URL:

<http://wrap.warwick.ac.uk/108228>

How to cite:

Please refer to published version for the most recent bibliographic citation information. If a published version is known of, the repository item page linked to above, will contain details on accessing it.

Copyright and reuse:

The Warwick Research Archive Portal (WRAP) makes this work by researchers of the University of Warwick available open access under the following conditions.

Copyright © and all moral rights to the version of the paper presented here belong to the individual author(s) and/or other copyright owners. To the extent reasonable and practicable the material made available in WRAP has been checked for eligibility before being made available.

Copies of full items can be used for personal research or study, educational, or not-for-profit purposes without prior permission or charge. Provided that the authors, title and full bibliographic details are credited, a hyperlink and/or URL is given for the original metadata page and the content is not changed in any way.

Publisher's statement:

Please refer to the repository item page, publisher's statement section, for further information.

For more information, please contact the WRAP Team at: wrap@warwick.ac.uk.

Modeling Duct Flow for Molecular Communication

Wayan Wicke*, Tobias Schwering*, Arman Ahmadzadeh*, Vahid Jamali*, Adam Noel[†], and Robert Schober*

*Institute for Digital Communications, Friedrich-Alexander-Universität Erlangen-Nürnberg

[†]School of Electrical Engineering and Computer Science, University of Ottawa

Abstract—Active transport is sought in molecular communication to extend coverage, improve reliability, and mitigate interference. One such active mechanism inherent to many liquid environments is fluid flow. Flow models are often over-simplified, e.g., assuming one-dimensional diffusion with constant drift. However, diffusion and flow are usually encountered in three-dimensional bounded environments where the flow is highly non-uniform such as in blood vessels or microfluidic channels. For a qualitative understanding of the relevant physical effects inherent to these channels a systematic framework is provided based on the Péclet number and the ratio of transmitter-receiver distance to duct radius. We review the relevant laws of physics and highlight when simplified models of uniform flow and advection-only transport are applicable. For several molecular communication setups, we highlight the effect of different flow scenarios on the channel impulse response.

I. INTRODUCTION

Using molecules for conveying digital messages has recently been recognized as a key communication strategy for nanoscale devices such as artificial cells cooperatively fighting a disease [1]. As the entities involved in this molecular communication are in the micro- and nanoscale, diffusion plays a significant role in the transport of messages [1].

However, diffusion has a limited effective range that renders molecular communication inefficient over extended distances. This limitation can be overcome by exploiting fluid flow in addition to diffusion. For example, in blood vessels it is the interplay of fluid flow and diffusion that governs the supply of oxygen from the lungs to tissues. Consequently, the molecular communication literature has considered basic models of these fundamental mechanisms [1]. In particular, the basic channel characteristics of diffusion in three-dimensional (3D) unbounded space with uniform flow in the context of molecular communication have been investigated for example in [2]. Such a model might be applicable when the boundaries are far from the nanonetwork. Our previous work [3] considered a 2D environment with uniform flow to study the impact of bounded drift-diffusion in more detail. On the other hand, 1D diffusion with drift has been studied in [4], [5]. It is not clear when such a simplified model is applicable in molecular communication since flow in blood vessels or in microfluidic channels, i.e., in ducts, especially at the microscale, is far from uniform [6], [7]. Hence, in general, a reduction of the 3D reality to a 1D model is not justified. In particular, the marginal axial and cross-sectional particle distributions are inherently coupled, which makes a mathematical analysis of the channel response difficult. This coupling has been considered in heuristic parametric models in [8] and simulated for blood vessels in [9].

The notion of dispersion as the interaction of diffusion and non-uniform laminar flow was principally investigated in [10], [11] and is now known as *Taylor dispersion* [6]. Via an *effective diffusion coefficient*, the particle distribution can be derived in the regime of large release-observation distances where the interaction of cross-sectional diffusion and non-uniform flow will have averaged to a uniform particle distribution in the cross-section and a Gaussian spread along the axis. For molecular communication, some authors adopted this model to keep their analysis analytically tractable but the conditions under which such simplifications are justified have not been considered in detail [12]–[16]. In particular, for short distances of the order of the duct radius, flow dominates as there has not been enough time for diffusion to affect the overall particle distribution. Recently, for molecular communication, this behavior which is in stark contrast to a diffusion regime, was also observed experimentally [17]. Thereby, the injection process determines the overall system response. There are several approaches to modeling the injection depending on the considered setup. One general first-order model of the injection is to consider a uniform initial distribution [18].

The focus of this paper is twofold. First, we introduce the notion of dispersion in a systematic manner which is in contrast to previous works. Second, we analyze and highlight the major effects of the advection-diffusion particle transport on molecular communication systems for two different regimes, namely the dispersion regime and the flow-dominated regime, the latter of which has not been considered in the molecular communication literature but is prevailing for example in blood vessels [6].

The two key messages of this paper are as follows:

- 1) There is a regime where one-dimensional diffusion with constant drift can accurately capture the channel characteristics by means of an effective diffusion coefficient and the cross-sectional mean velocity. In this regime, the initial spatial release pattern at the transmitter does not affect the resulting particle distribution.
- 2) Non-uniform flow as encountered in ducts can cause significant intersymbol interference (ISI), especially in a flow-dominated regime. Diffusion tends to decrease long-term ISI by enabling slowly-moving particles to move away from the boundary.

This paper is structured as follows. In Section II, we introduce the system model and present preliminaries. Section III analyzes the duct channel and the different flow regimes. Numerical results are presented in Section IV. Finally, in Section V, we draw some conclusions.

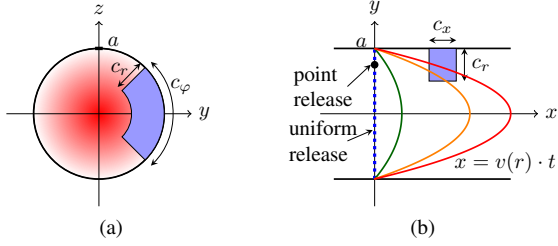


Fig. 1. System model geometry (a) in the cross-section, and (b) along the axis. The red shading in (a) reflects the flow velocity which is maximum in the center and vanishes at the boundary. The corresponding parabolic shape, $x = v(r) \cdot t$, on which released particles reside when not diffusing after a uniform release, is sketched in (b) for three different time instances. Point and uniform transmitter release are shown as black dot and as a blue line, respectively.

II. SYSTEM MODEL AND PRELIMINARIES

A. System Model

We consider a straight impermeable cylindrical duct of infinite axial extent and radius a which can be described in cylindrical coordinates by the points (x, r, φ) , where $x \in (-\infty, \infty)$ is the axial position, $r \in [0, a]$ is the radial distance, and $\varphi \in (-\pi, \pi]$ is the azimuth angle. The duct is filled with a fluid of viscosity η that is subject to steady laminar flow in the x -direction where the flow velocity $v(r)$ is a function of r only and is given by a parabolic function; see Fig. 1.

We consider a transmitter (TX) that releases N_{TX} molecules via on-off keying (OOK) either 1) uniformly and *randomly* distributed over the cross section at $x = 0$, or 2) from the point $(0, r_0, \varphi_0)$. Moreover, we assume a transparent receiver (RX) specified by the points (x, r, φ) satisfying $|x - d| \leq c_x/2$, $a - c_r \leq r \leq a$, $|\varphi| \leq c_\varphi/2$, i.e., the receiver is mounted on the duct wall with axial TX-RX distance given by d , radial extent c_r , and spanning an angle of c_φ (see Fig. 1). Detection of the OOK symbols $a[k] \in \{0, 1\}$ is performed based on the number of observed particles $N_{\text{ob}}(t)$ by applying a threshold $\xi \in \{0, 1, \dots, N_{\text{TX}}\}$:

$$\hat{a}[k] = \begin{cases} 0, & N_{\text{ob}}(t_0 + kT) < \xi \\ 1, & N_{\text{ob}}(t_0 + kT) \geq \xi, \end{cases} \quad (1)$$

where t_0 is a detection delay and $\hat{a}[k]$ is the detected OOK symbol in the k -th symbol interval of length T , i.e., for OOK $1/T$ is the data rate.

We model the particle release from the TX as instantaneous and the released particles are transported by the fluid flow and Brownian motion. For simplicity, we assume that particles do not interact with each other nor influence the flow field. Because of their small size, other forces such as gravity acting on the particles are negligible [7].

B. Preliminaries

In molecular communication, information is conveyed by mass transfer. Mass transfer in fluids is mediated by flow and Brownian motion which is referred to as *advection* and *diffusion*, respectively. Thereby, mass transfer can be described

by a time-varying spatial probability density function (PDF) $p(\mathbf{r}; t)$ which can be interpreted as a normalized concentration where $dV \cdot p(\mathbf{r}; t)$ gives the average fraction of particles within the differential volume dV at \mathbf{r} at time t . The PDF $p(\mathbf{r}; t)$ can be found as the solution to the following partial differential equation (PDE), which we will also refer to as the advection-diffusion equation [7, Eq. (5.22)]

$$\partial_t p = D \nabla^2 p - \nabla \cdot p \mathbf{v}, \quad (2)$$

where $\partial_t p = \frac{\partial}{\partial t} p$ denotes the partial derivative of p with respect to t and ∇ is the Nabla operator. Moreover, D is the diffusion coefficient and $\mathbf{v}(\mathbf{r})$ is the velocity vector at point \mathbf{r} .

To solve (2), we need to know the velocity field $\mathbf{v}(\mathbf{r})$. In general, the velocity field can be obtained by solving the Navier-Stokes equation, which provides a fundamental description of flow by relating the velocity field to the local pressure [7, Ch. 2]. Applied to rigid and straight channels with no-slip boundary conditions, i.e., where the velocity at the boundary is zero, and subject to pressure-driven flow in the steady-state, the velocity profile is referred to as *Poiseuille flow* [7, Ch. 3]. Thereby, assuming a *Newtonian fluid*, i.e., a fluid which can be described by the viscosity η , we obtain [7, Eq. (3.32)]

$$v(r) = 2v_{\text{eff}} \left(1 - \frac{r^2}{a^2} \right), \quad (3)$$

where v_{eff} is the mean velocity in the channel and is a function of the applied pressure gradient $\partial_x P$. In particular, v_{eff} can be obtained as [7, Eq. (3.34)]

$$v_{\text{eff}} = \frac{|\partial_x P| a^2}{8\eta}.$$

We note that the maximum velocity $v_{\text{max}} = 2v_{\text{eff}}$ occurs at the center and can be found using $r = 0$ in (3).

An important parameter is the Péclet number, which gives an estimate of the importance of diffusion over advection. This dimensionless number is defined as [6, Eq. (4.6.8)]

$$\text{Pe} = \frac{v_{\text{eff}} a}{D}, \quad (4)$$

when considering the duct radius a as the length scale of interest. Intuitively, $\text{Pe} \in [0, \infty)$ increases and decreases when v_{eff} and D increase as the importance of particle transport by flow and diffusion becomes more relevant, respectively.

III. ANALYSIS OF THE DUCT CHANNEL

The advection-diffusion equation (2) for the environment in Fig. 1 simplifies to the following PDE:

$$\partial_t p = D \nabla^2 p - v(r) \partial_x p, \quad (5)$$

for $t > 0$ because the velocity field is independent of the axial position. At the boundary $r = a$, $\partial_r p = 0$ has to hold and $p(x, r, \varphi; 0)$ is initially given by $\delta(x)/(\pi a^2)$ and $\delta(x)\delta(r - r_0)\delta(\varphi - \varphi_0)/r$ for uniform and point release, respectively. Eq. (5) is still difficult to solve in general because of the nonlinear velocity (3) and the inherent coupling of p in the x - and r -directions. Interestingly, (5) can be solved in a quasi-steady-state where enough time has passed such that

cross-sectional diffusion and the non-uniform flow profile have averaged out. We will refer to this behavior as the *dispersion regime*. Trivially, this regime includes the special case where $v_{\text{eff}} \rightarrow 0$, i.e., when there is *pure diffusion*. Another special case where (5) can be solved is when $D \rightarrow 0$, i.e., when we are in the *flow-dominated regime*.

For each of these regimes, we seek the time-dependent observation probability

$$P_{\text{ob}}(t) = \int_{V_{\text{RX}}} p(x, r, \varphi; t) dV_{\text{RX}}, \quad (6)$$

where V_{RX} is the RX volume. We will also refer to $P_{\text{ob}}(t)$ as the *impulse response* of the molecular communication channel. The impulse response is a fundamental characteristic of the molecular communication channel as it determines the mean $\overline{N_{\text{ob}}}(t)$ of the received signal [2] $N_{\text{ob}}(t)$

$$\overline{N_{\text{ob}}}(t) = N_{\text{TX}} \sum_{k=0}^{\infty} a[k] P_{\text{ob}}(t - kT) + N_{\text{n}}, \quad (7)$$

where N_{n} is external noise. We note that in general $N_{\text{ob}}(t)$ is a binomial random variable which can be approximated by a Poisson random variable of mean $\overline{N_{\text{ob}}}(t)$ [2]. Based on this assumption also the symbol error rate (SER) can be determined which, as performance measure, we will evaluate in Section IV.

A. Dispersion Regime

Dispersion is the result of the interaction of cross-sectional diffusion and the non-uniform advection due to the flow profile. This interaction can lead to a particle distribution that is uniform in each cross-section, i.e., the spatial PDF can be written as $p(x, r, \varphi; t) = p(x; t)/(\pi a^2)$. In this regime, the particle distribution does depend only on the initial x -position, i.e., there is no difference for point and uniform release. This behavior occurs if [6, Chapter 4.6]

$$\text{Pe} \ll 4 \frac{d}{a}, \quad (8)$$

e.g., when the TX-RX distance is large, the diffusion coefficient is large, or the duct radius is small. Naturally, this includes the special case of pure diffusion where flow is not present. If (8) is satisfied, (5) can be written as the following 1D advection-diffusion equation [6, Eq. (4.6.30)]

$$\partial_t p = D_{\text{eff}} \partial_x^2 p - v_{\text{eff}} \partial_x p, \quad (9)$$

with *effective diffusion coefficient* D_{eff} and mean velocity v_{eff} . For an instantaneous uniform release at $x = 0$, the solution to (9) is given by

$$p(x, r, \varphi; t) = \frac{1}{\pi a^2} \times \frac{1}{\sqrt{4\pi D_{\text{eff}} t}} \exp\left(-\frac{(x - v_{\text{eff}} t)^2}{4D_{\text{eff}} t}\right), \quad (10)$$

where $1/(\pi a^2)$ is the cross-sectional distribution in the r - and φ -directions.

Following [11, Eq. (26)], the *Taylor-Aris* effective diffusion coefficient D_{eff} is obtained as [6, Eq. (4.6.35)]

$$D_{\text{eff}} = D \left(1 + \frac{1}{48} \text{Pe}^2\right). \quad (11)$$

We note that in general $D_{\text{eff}} > D$ and moreover $D_{\text{eff}} \gg D$ when D is decreased to very small values, which by (4) increases Pe . However, by (8), decreasing D comes at the expense of a larger required distance for dispersion to take place. In fact, we can rearrange (8) as

$$D \gg \frac{a^2 \cdot v_{\text{eff}}}{4d}, \quad (12)$$

which approximates the minimum diffusion coefficient required for dispersion to occur. For small and large D , we can neglect the first and second parts in the sum on the right-hand side of (11), respectively.

The observation probability obtained by integrating (10) over the receiver volume is given by (6)

$$P_{\text{ob,d}}(t) = \frac{A_{\text{RX}}}{a^2} \times \left[\text{Q}\left(\frac{d - c_x/2 - v_{\text{eff}} t}{2D_{\text{eff}} t}\right) - \text{Q}\left(\frac{d + c_x/2 - v_{\text{eff}} t}{2D_{\text{eff}} t}\right) \right], \quad (13)$$

where $\text{Q}(\cdot)$ is the Gaussian Q-function and $A_{\text{RX}} = c_\varphi/(2\pi) \cdot (2ac_r - c_r^2)$ is the surface area of the RX in the cross section.

It is of interest to derive the time at which $P_{\text{ob,d}}(t)$ attains its maximum as this may serve as design guideline for the symbol interval length. As maximizing $P_{\text{ob,d}}(t)$ with respect to t is cumbersome, we resort to maximizing (10) for $x = d$, which yields

$$t_{\text{max}} = \frac{D_{\text{eff}}}{v_{\text{eff}}^2} \left(-1 + \sqrt{1 + \frac{v_{\text{eff}}^2}{D_{\text{eff}}^2} d^2}\right). \quad (14)$$

In this approximation, the peak height follows as $p_{\text{max}} = P_{\text{ob,d}}(t_{\text{max}})$. We note that because of diffusion $t_{\text{max}} < d/v_{\text{eff}}$, where d/v_{eff} is the time when particles moving with the mean velocity will reach the RX.

B. Flow-dominated Regime

In this subsection, we directly determine the observation probability $P_{\text{ob,f}}(t) = P_{\text{ob}}(t)$ by neglecting diffusion and without resorting to (6).

1) *Uniform Release*: First, we assume a uniform release at $x = 0$. In this case, all particles will lie on the surface of a paraboloid that extends along the axis over time and exhibits rotational symmetry. Thereby, the marginal distribution in the cross-section, i.e., for the r - and φ -coordinates, remains uniform because the flow is in the x -direction. The geometric shape is given by $x = v(r) \cdot t$, cf. Fig. 1. Hence, the time t when the points (x, r, φ) lie on the paraboloid is simply given by $t = x/v(r)$. From this, we also obtain the following auxiliary relationship:

$$r_t(x) = a \cdot \sqrt{1 - \frac{x}{2v_{\text{eff}} t}}, \quad (15)$$

which is obtained by re-arranging (3).

The fraction of particles within the receiver volume is determined by those particles that lie within a segment of angular extent c_φ and within a ring-region with inner and outer radii $r_i(t)$ and $r_o(t)$, respectively. Following the uniform release

at $x = 0$, the observation probability $P_{\text{ob},f}(t)$ can consequently be written as $P_{\text{ob},f}(t) = c_\varphi/(2\pi) \cdot (r_o^2 - r_i^2)/a^2$. Variables $r_i(t)$ and $r_o(t)$ depend on how the paraboloid intersects with the RX volume. In fact, there are three scenarios, which are shown in Fig. 1b for the x - y -plane. In the first case, the paraboloid has not yet reached the RX, cf. the green line in Fig. 1b. The first intersection occurs at $t = t_1$ when the paraboloid reaches the points $(x = d - c_x/2, r = a - c_r, \varphi)$ where $\varphi \in [-c_\varphi/2, c_\varphi/2]$. In the second case, for $t_1 < t < t_2$, the paraboloid intersects with the RX at $r_i(t) = a - c_r$ and $r_o(t) = r_t(d - c_x/2)$, cf. the orange line in Fig. 1b. Time t_2 is characterized by the paraboloid intersecting with the RX at the points $(d + c_x/2, a - c_r, \varphi)$ where $\varphi \in [-c_\varphi/2, c_\varphi/2]$. The last case occurs for $t \geq t_2$, cf. the red line in Fig. 1b. In this case, we have $r_i(t) = r_t(d - c_x/2)$ and $r_o(t) = r_t(d + c_x/2)$. Now, we only require t_1 and t_2 in order to obtain the impulse response. From $x = v(r) \cdot t$ and (3), we obtain

$$t_{1,2} = \frac{d \mp c_x/2}{2v_{\text{eff}}(1 - (1 - c_r/a)^2)} \quad (16)$$

In summary, the impulse response in the flow-dominated regime following a uniform release can be written as

$$P_{\text{ob},f}(t) = \begin{cases} 0, & t \leq t_1 \\ \left[\frac{1}{a^2} A_{\text{RX}} - \frac{c_\varphi}{2\pi} \frac{d - c_x/2}{2v_{\text{eff}}t} \right], & t_1 < t < t_2 \\ \frac{c_\varphi}{2\pi} \cdot \frac{c_x}{2v_{\text{eff}}t}, & t \geq t_2. \end{cases} \quad (17)$$

$P_{\text{ob},f}(t)$ is maximized for $t = t_2$. Also, at time $t = t_2/\alpha$ the fraction $\alpha \in (0, 1]$ of $P_{\text{ob},f}(t_2)$ can be observed. The tail of the impulse response decays only polynomial with time, which may give rise to significant ISI in molecular communication systems.

2) *Point Release*: For a point release with $r_0 \in [a - c_r, a]$ and $\varphi_0 \in [-c_\varphi/2, c_\varphi/2]$, i.e., when the TX coordinates are within the r - and φ -coordinates of the RX, we observe all particles with certainty if $d - c_x/2 \leq v(r_0)t \leq d + c_x/2$, i.e., the impulse response is given by

$$P_{\text{ob},f}^\bullet(t) = \text{rect}\left(\frac{v(r_0)t - d}{c_x}\right), \quad (18)$$

where $\text{rect}(x) = 1$ if $-1/2 \leq x \leq 1/2$ and zero otherwise. When the release point is *not* within the r - and φ -coordinates of the RX then the impulse response is zero for all times.

Eqs. (17) and (18) are intuitively valid when $D \rightarrow 0$. More generally, the solution is applicable when $\text{Pe} \gg d/a$ [6], e.g., when the duct radius is large or the TX-RX distance is small.

We note that (17) and (18) still give the observation probability $\in [0, 1]$ even though the flow is deterministic, i.e., with probability $P_{\text{ob}}(t)$ and $1 - P_{\text{ob}}(t)$ each of the N_{TX} particles can be independently and cannot be observed within the RX volume at time t , respectively. The reason for this is that for both uniform and point release the initial particle position can be understood as independently and uniformly random distributed within the available TX area (the whole cross section or one point).

IV. NUMERICAL EVALUATION

By using particle-based simulation, we validate our derived analytical expressions and explore those regimes for which mathematical analysis is not readily accomplished. Thereby, unless explicitly stated otherwise, we employ the following physical parameter values. As diffusion coefficient we choose $D = 10^{-10} \text{ m}^2/\text{s}$ which is a reasonable estimate for small proteins [6]. Two values for the duct radius $a = 10 \mu\text{m}$ and $a = 200 \mu\text{m}$ are considered, which is reasonable for small capillaries [6] and microfluidic ducts [7], respectively. Thereby, two TX-RX distances are considered with values $d = 200 \mu\text{m}$ and $d = 800 \mu\text{m}$. Moreover, we choose the receiver dimensions as $c_x = a/2$, $c_r = a/2$, $c_\varphi = \pi/2$, i.e., the receiver size scales with the duct radius. The microscopic simulation time step is set to $\Delta t = 10^{-3} \text{ s}$. The fluid flow mean velocity is assumed to be $v_{\text{eff}} = 1 \text{ mm s}^{-1}$, which is reasonable for small capillaries [6].

For $a = 10 \mu\text{m}$, for $D = 10^{-10} \text{ m}^2/\text{s}$, we obtain $D_{\text{eff}} = 2.1 \times 10^{-8} \text{ m}^2/\text{s}$, which is a value otherwise unattainable for the diffusion coefficient of small proteins [6]. For $a = 50 \mu\text{m}$ and $a = 200 \mu\text{m}$, for $D = 10^{-10} \text{ m}^2/\text{s}$ and $d = 800 \mu\text{m}$ by (12) D_{eff} is not meaningful anymore, cf. Fig. 2.

We show in Fig. 2 (adapted from [6]) the considered parameter values in terms of the Péclet number and the ratio of the TX-RX distance to the duct radius. In particular, we have shaded the two regimes for which the obtained analytical results from Section III are expected to be applicable. Eq. (8) separates these two regimes and is shown as black line. The derived analytical results are valid for parameter values well within the dispersion or the flow-dominated regime. However, the analytical results cannot be expected to be accurate close to the boundary set by (8). For the two duct radii $a = 10 \mu\text{m}$, $200 \mu\text{m}$ and the two TX-RX distances $d = 200 \mu\text{m}$, $800 \mu\text{m}$, we show the resulting four combinations of d/a and Pe as black dots in Fig. 2. We see that the two scenarios for $a = 10 \mu\text{m}$ lie close to the boundary of both regions. These parameter values have been chosen such that simulations can reveal the deviations from either regime. On the other hand, the scenarios for $a = 200 \mu\text{m}$ lie well within the flow-dominated regime and we expect no deviations from the developed theory. We note that changing the duct radius a affects both d/a and Pe whereas a change in d influences only d/a . Considering the parameter values chosen in this paper, from Fig. 2, we can conclude that the dispersion regime is most applicable for small microscale ducts. On the other hand, we also see that there is a large set of parameters for which the flow-dominated regime is more appropriate, especially for medium to large ducts.

To gain a basic understanding of the particle evolution towards dispersion, in Fig. 3, we show three snapshots of the particle positions corresponding to three different time instances and distinguished by different colors following a uniform release at $t = 0$. In particular, we plot r^2 over x motivated by the fact that the marginal distribution in r^2 of a uniform distribution within a circular disk is uniform. As a side effect, for the flow-dominated regime from (15), r^2 becomes a simple linear function which for each considered

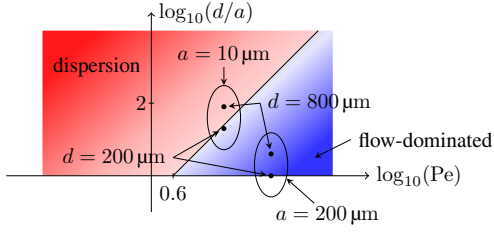


Fig. 2. Sketch of regions of different transport regimes. Adapted from [6]. All four simulation scenarios are shown as black dots. For $a = 10 \mu\text{m}$, we have $\text{Pe} = 100$ and $d/a = 20, 80$. For $a = 200 \mu\text{m}$, we have $\text{Pe} = 2000$ and $d/a = 1, 4$.

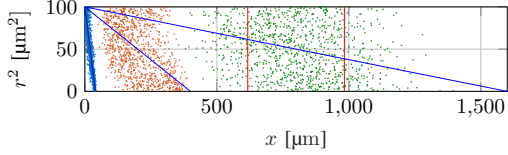


Fig. 3. Snapshot of particle positions for $a = 10 \mu\text{m}$ and at $t = 0.02, 0.2, 0.8 \text{ s}$ after uniform release at $x = 0$ and $t = 0$ shown in different colors and starting from left to right, respectively. In total, $N_{\text{TX}} = 10^3$ are released.

t is shown as a blue line. Furthermore, $a = 10 \mu\text{m}$ such that according to Fig. 2, dispersion occurs for x in the vicinity of $d = 800 \mu\text{m}$. For the largest time shown, $t = 0.8 \text{ s}$, the red lines show the standard deviation positions $v_{\text{eff}}t \pm \sqrt{2D_{\text{eff}}t}$ from the mean when assuming the Gaussian distribution in (10) due to dispersion. For small times, e.g., $t = 0.02 \text{ s}$, the particles follow the parabolic profile (15) closely. For slightly larger times, e.g., $t = 0.2 \text{ s}$, the particles start to spread because of diffusion. For large times, e.g., $t = 0.8 \text{ s}$, particles become uniformly distributed along the r^2 dimension within the duct due to dispersion. We note that for $v_{\text{eff}} = 1 \text{ mm s}^{-1}$, at $t = 0.2 \text{ s}$ and $t = 0.8 \text{ s}$, the mean particle position has arrived at $d = 200 \mu\text{m}$ and $d = 800 \mu\text{m}$, respectively. In summary, at small times after the release the flow-dominated regime and at large times after the release the dispersion regime accurately model the actual behavior.

In Figs. 4a and 4b, we show the impulse response for $a = 10 \mu\text{m}$ and $a = 200 \mu\text{m}$, respectively. In each case, we consider both $d = 200 \mu\text{m}$ and $d = 800 \mu\text{m}$ as well as uniform and point release. For the point release, the position $(0, 0.75a, 0)$ was chosen such that particles can arrive at the receiver when not diffusing. We simulate the impulse responses and investigate which of the developed analytical models provides the best fit in each case.

In Fig. 4a, for comparison, both $P_{\text{ob},d}(t)$ (applicable for both point and uniform release) in (13) and $P_{\text{ob},f}(t)$ (applicable only for uniform release) in (17) are shown. Thereby, for $P_{\text{ob},d}(t)$, the peaks via (14) are also highlighted with large dots. When $d = 200 \mu\text{m}$, the simulated impulse response following a point release is significantly larger than that for a simulated uniform release. In this case, both simulated impulse responses neither match $P_{\text{ob},d}(t)$ nor $P_{\text{ob},f}(t)$. However, especially considering the long-time behavior, e.g., for $t > 0.5 \text{ s}$, the simulated data points tend to be better described by $P_{\text{ob},d}(t)$ than by $P_{\text{ob},f}(t)$. For $d = 800 \mu\text{m}$, the deviations of the simulated impulse

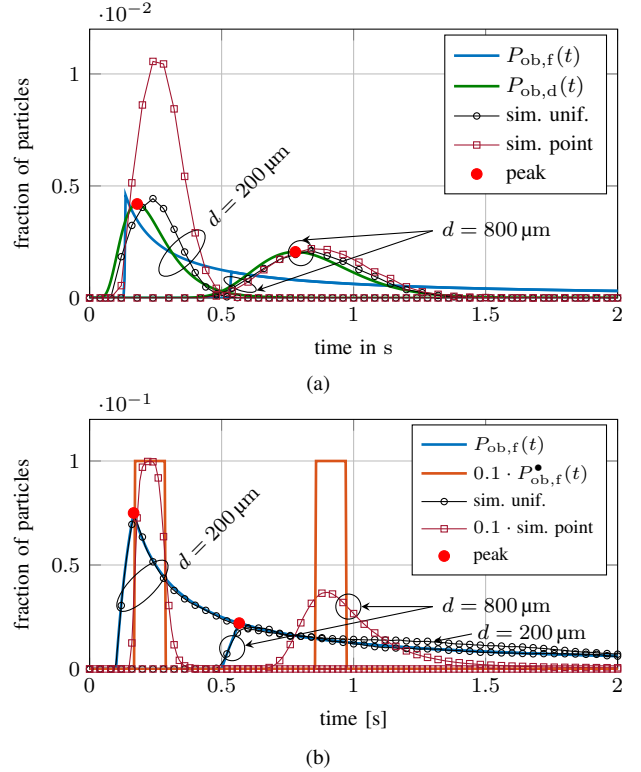


Fig. 4. Impulse responses for (a) $a = 10 \mu\text{m}$, and (b) $a = 200 \mu\text{m}$. Simulation results are shown for both uniform and point release. For (b), additionally the simulated and analytical impulse responses due to a point release are scaled by the constant factor 0.1 for a better visualization. Simulation results are for $N_{\text{TX}} = 10^6$.

responses for point and uniform release from $P_{\text{ob},d}(t)$ are much smaller and the dispersion regime provides a much better fit despite the fact that (8) is not strictly satisfied, cf. Fig. 2. This is consistent with the green particle cloud in Fig. 3 which appears uniform in r^2 . Comparing $P_{\text{ob},f}(t)$ and $P_{\text{ob},d}(t)$, we see that the peak of $P_{\text{ob},f}(t)$ is larger and smaller than that of $P_{\text{ob},d}(t)$ when d is small and large, respectively. For larger times, e.g., for $t > 0.75 \text{ s}$, $P_{\text{ob},f}(t)$ for $d = 200 \mu\text{m}$ and $P_{\text{ob},f}(t)$ for $d = 800 \mu\text{m}$ coincide as expected from (17) which is independent of d for $t > t_2$. In conclusion, parameter values close to the boundary in Fig. 2 can still be applicable for the dispersion model.

In Fig. 4b, $P_{\text{ob},f}(t)$ in (17) and $P_{\text{ob},f}^*(t)$ in (18) are shown. For the former, the peak times t_2 are highlighted. For both uniform and point release, simulation results are also shown. By Fig. 2, the dispersion approximation is not applicable in this scenario and for clarity is not shown. Considering the point release, the simulated curve for $d = 200 \mu\text{m}$ matches the rectangular shape of $P_{\text{ob},f}^*(t)$ in (18) reasonably well. On the other hand, for $d = 800 \mu\text{m}$, the simulated impulse response significantly deviates from the rectangular shape because diffusion has had enough time to result in a spread of the pulse. As expected from Fig. 2, we observe in general a good agreement between $P_{\text{ob},f}(t)$ in (17) and the simulation results in the case of a uniform release, i.e., the flow-dominated regime provides a reasonable description of the channel. Nevertheless, for $d = 200 \mu\text{m}$, at larger times, e.g., for $t > 1 \text{ s}$, there is

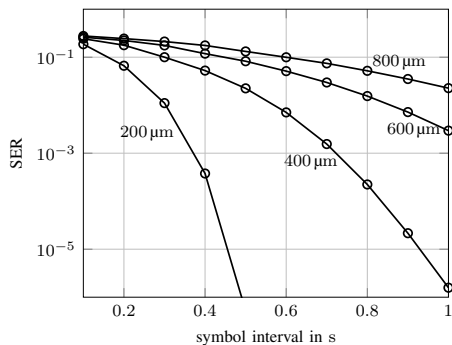


Fig. 5. Symbol error rate as a function of the symbol interval length for $d = 200, 400, 600, 800 \mu\text{m}$. Parameters are chosen as $N_{\text{TX}} = 10^4$, $N_{\text{n}} = 10$.

a small deviation because of residual particles close to the RX when most particles have already passed. Comparing the impulse responses for point release and uniform release, we find that the tail of the impulse response strongly depends on the initial distribution. There can be considerable ISI, especially when a fraction of the particles is released close to the duct wall. However, as long as the RX can be reached by the particles, an initial release close to the center of the duct might reduce ISI.

Comparing Figs. 4a and 4b, we see that the channels behave completely different when the duct radius is changed from $a = 10 \mu\text{m}$ to $a = 200 \mu\text{m}$. We note that for both uniform and point release the peak values of the impulse responses in Fig. 4a are at least by an order of magnitude smaller than in Fig. 4b. Moreover, for uniform and point release the simulated impulse responses in Fig. 4a decay faster and slower from their peak values than those in Fig. 4b, respectively.

In Fig. 5, we show the average SER for OOK modulation of maximally 8 interfering symbols and threshold detection of the detected number of transmitted particles as a function of the symbol interval length using the analytic impulse response in (17) for the flow-dominated regime. The curves are parameterized by the TX-RX distance d , which is varied from $200 \mu\text{m}$ to $800 \mu\text{m}$. As detection time offset, i.e., as delay, $t_0 = t_2$ is chosen and an average of 10 noise molecules is assumed. For each considered symbol interval and TX-RX distance, the minimum SER over the threshold ξ is found by full search. In general, the SER decreases for increasing T at the expense of decreasing the data rate $1/T$. However, for moderate to large distances, e.g., $d = 800 \mu\text{m}$, the SER does not decrease significantly even if the symbol interval is taken very large, e.g., $T = 1 \text{ s}$, because of severe ISI, cf. Fig. 4b. The supported distance for a maximally tolerated SER could potentially be increased by adapting the injection mechanism as can drastically be seen by the rectangular-shape impulse response for a point release in Fig. 4b. On the other hand, additional processing of the received signal before detection such as differentiating the received signal might also enhance the performance.

V. CONCLUSION

Dispersion generalizes the concept of diffusion which is crucial for signal propagation in molecular communication.

Thereby, a non-uniform flow can be accounted for by an effective diffusion coefficient. This effective diffusion coefficient can be multiple orders of magnitude larger than the molecular diffusion coefficient. However, this description relies on a large TX-RX distance. On the other hand, there are many practical scenarios at the microscale that fall within a flow-dominated regime where dispersion is insignificant. In this regime, the initial release pattern drastically influences ISI. For a given duct radius either regime can be applicable depending on the TX-RX distance and the Péclet number.

REFERENCES

- [1] N. Farsad, H. B. Yilmaz, A. Eckford, C. B. Chae, and W. Guo, "A comprehensive survey of recent advancements in molecular communication," *IEEE Commun. Surv. Tutorials*, vol. 18, no. 3, pp. 1887–1919, 2016.
- [2] A. Noel, K. C. Cheung, and R. Schober, "Optimal receiver design for diffusive molecular communication with flow and additive noise," *IEEE Trans. Nanobioscience*, vol. 13, no. 3, pp. 350–362, Sep. 2014.
- [3] W. Wicke, A. Ahmadzadeh, V. Jamali, H. Unterweger, C. Alexiou, and R. Schober, "Molecular communication using magnetic nanoparticles," *arXiv:1704.04206*, Accept. for Present. IEEE WCNC 2018.
- [4] K. V. Srinivas, A. W. Eckford, and R. S. Adve, "Molecular communication in fluid media: The additive inverse Gaussian noise channel," *IEEE Trans. Inf. Theory*, vol. 58, no. 7, pp. 4678–4692, Jul. 2012.
- [5] N. R. Kim, A. W. Eckford, and C. B. Chae, "Symbol interval optimization for molecular communication with drift," *IEEE Trans. Nanobioscience*, vol. 13, no. 3, pp. 223–229, Sep. 2014.
- [6] R. F. Probstein, *Physicochemical Hydrodynamics: An Introduction*. John Wiley & Sons, Feb. 2005.
- [7] H. Bruus, *Theoretical Microfluidics*, 1st ed. Oxford University Press, Nov. 2007.
- [8] M. Kucsu and O. B. Akan, "Modeling convection-diffusion-reaction systems for microfluidic molecular communications with surface-based receivers in internet of bio-nano things," *PLoS One*, vol. 13, no. 2, p. e0192202, 2018.
- [9] L. Felicetti, M. Femminella, and G. Reali, "Simulation of molecular signaling in blood vessels: Software design and application to atherosclerosis," *Nano Commun. Networks*, vol. 4, no. 3, pp. 98–119, Sep. 2013.
- [10] G. I. Taylor, "Dispersion of soluble matter in solvent flowing slowly through a tube," *Proc. R. Soc. Lond. A*, vol. 219, no. 1137, pp. 186–203, Aug. 1953.
- [11] R. Aris, "On the dispersion of a solute in a fluid flowing through a tube," *Proc. R. Soc. Lond. A*, vol. 235, no. 1200, pp. 67–77, Apr. 1956.
- [12] P. He, Y. Mao, Q. Liu, P. Li, and K. Yang, "Channel modelling of molecular communications across blood vessels and nerves," in *Proc. IEEE ICC 2016*, May 2016, pp. 1–6.
- [13] Y. Chahibi, M. Pierobon, and I. F. Akyildiz, "Pharmacokinetic modeling and biodistribution estimation through the molecular communication paradigm," *IEEE Trans. Biomed. Eng.*, vol. 62, no. 10, pp. 2410–2420, Oct. 2015.
- [14] A. O. Bicen and I. F. Akyildiz, "System-theoretic analysis and least-squares design of microfluidic channels for flow-induced molecular communication," *IEEE Trans. Signal Process.*, vol. 61, no. 20, pp. 5000–5013, Oct. 2013.
- [15] Y. Sun, K. Yang, and Q. Liu, "Channel capacity modelling of blood capillary-based molecular communication with blood flow drift," in *Proc. ACM NanoCom 2017*, 2017, pp. 19:1–19:6.
- [16] A. O. Bicen, J. J. Lehtomäki, and I. F. Akyildiz, "Shannon meets Fick on the microfluidic channel: diffusion limit to sum broadcast capacity for molecular communication," *IEEE Trans. Nanobiosci.*, vol. 17, no. 1, pp. 88–94, 2018.
- [17] H. Unterweger, J. Kirchner, W. Wicke, A. Ahmadzadeh, D. Ahmed, V. Jamali, C. Alexiou, G. Fischer, and R. Schober, "Experimental molecular communication testbed based on magnetic nanoparticles in duct flow," *arXiv preprint arXiv:1803.06990*, 2018.
- [18] O. Levenspiel, *Chemical reaction engineering*, 3rd ed. John Wiley & Sons, 1999.